Demonstration of three-dimensional optical imaging using a confocal microscope based on a liquid-crystal electronic lens

Nabeel A. Riza
Mumtaz Sheikh
University of Central Florida
CREOL, College of Optics & Photonics
Photonic Information Processing Systems (PIPS) Laboratory
4000 Central Florida Boulevard
Orlando, Florida 32816-2700
E-mail: riza@creol.ucf.edu

Grady Webb-Wood
Pieter G. Kik
University of Central Florida
CREOL, College of Optics & Photonics
Nano-Photonics and Near Field Optics Laboratory
4000 Central Florida Boulevard
Orlando, Florida 32816-2700

Abstract. Three-dimensional (3-D) imaging is demonstrated using an electronically controlled liquid crystal (LC) optical lens to accomplish a no-moving-parts depth-section scanning in a modified commercial 3-D confocal microscope. Specifically, 3-D views of a standard CDC blood vessel (enclosed in a glass slide) have been obtained using the modified confocal microscope operating at the red 633-nm laser wavelength. The image sizes over a 25-μm axial scan depth were 50×50 μm and 80×80 μm, using $60\times$ and $20\times$ micro-objectives, respectively. The transverse motion step was 0.1 μm for the $60\times$ data and 0.2 μm for the $20\times$ data. As a first-step comparison, image processing of the standard and LC electronic-lens microscope images indicates correlation values between 0.81 and 0.91. The proposed microscopy system within aberration limits has the potential to eliminate the mechanical forces due to sample or objective motion that can distort the original sample structure and lead to imaging errors. © *2008 Society of Photo-Optical Instrumentation Engineers.* [DOI: 10.1117/1.2944135]

Subject terms: Liquid crystal; optical imaging; microscopy.

Paper 080096 received Feb. 1, 2008; accepted for publication Mar. 24, 2008; published online Jul. 2, 2008.

1 Introduction

Confocal microscopes are widely used for 3-D imaging of microscopic objects. In the basic confocal microscope, a point source is focused onto the sample, using an objective lens. The reflected or transmitted light, depending on which configuration is used, is collected by the same or a different objective lens and focused on a tiny pinhole in front of the detector, using a spherical lens. The size of the pinhole is chosen to let only the central part of the Airy pattern hit the detector. This ensures that only the rays coming from the image focal plane can reach the detector while all the out-of-focus light is rejected. This confocal process strongly increases image contrast and hence is a powerful tool to implement 3-D imaging.[1–4] The confocal process also vastly reduces background fluorescence from out-of-focus parts of the sample, which cannot be done in standard optical microscopy.

Most present-day confocal microscopes use a combination of mirror-based beam scanning for transverse (xy) beam motion and piezoelectric mechanical motion of sample stage or objective to achieve z-direction (axial) scans to complete data acquisition for 3-D imaging of test samples. Because piezoelectric stages have inherent hysteresis, the system uses complex feedback controls to maintain scan motion operational accuracy. Fast axial mechanical motion of the objective or the sample, which are typically coupled via an index-matching fluid (e.g., oil), can cause mechanical forces to develop within the sample structure, particularly a live sample. Hence, it would be highly useful to remove these axial-motion-produced mechanical forces on a sample by using an electronic lens (e-lens) to electronically change the axial focus position on a sample. Ultimately, one should be able to deploy no-moving-parts optical scanners within the microscope system to enable a 3-D scanning optical beam on the specimen under observation.

The scanning operation can move a beam focus in one (linear), two (transverse), or three (transverse+axial) dimensions. For example, the use of multiple wavelengths coupled with dispersive media to implement optical beam scanning goes back to laser radar designs in 1971.[5] The subsequent use of a chromatic lens with wavelength encoding for axial scans dates back to 1984 for profilometry,[6,7] and the same concept was later used for microscopy designs.[8,9] Use of multiple wavelengths for spatial phased-array mapping at the exit of a single-mode fiber (SMF) for biomedical ultrasonic ultracompact probe design was introduced in 1995.[10,11] Further extensions of the wavelength-to-space mapping concepts occurred for designing no-moving-parts microscopes with one-dimensional (1-D) scanning (stare mode)[12–17] and two-dimensional (2-D) optical scanning and for designing free-space laser communication systems.[18,19] Although this design is elegant and highly useful for intracavity applications,[20,21] the wavelength encoding of a beam's spatial properties assumes the beam-sample interaction to be uniform and furthermore puts broadband performance constraints on all optics used to make the scanning microscope. Hence, a wavelength-insensitive optical scanning design such as traditional scanning mirrors coupled with sample (or objective) motion is preferred today. Nevertheless, next-generation electroni-

0091-3286/2008/$25.00 © 2008 SPIE

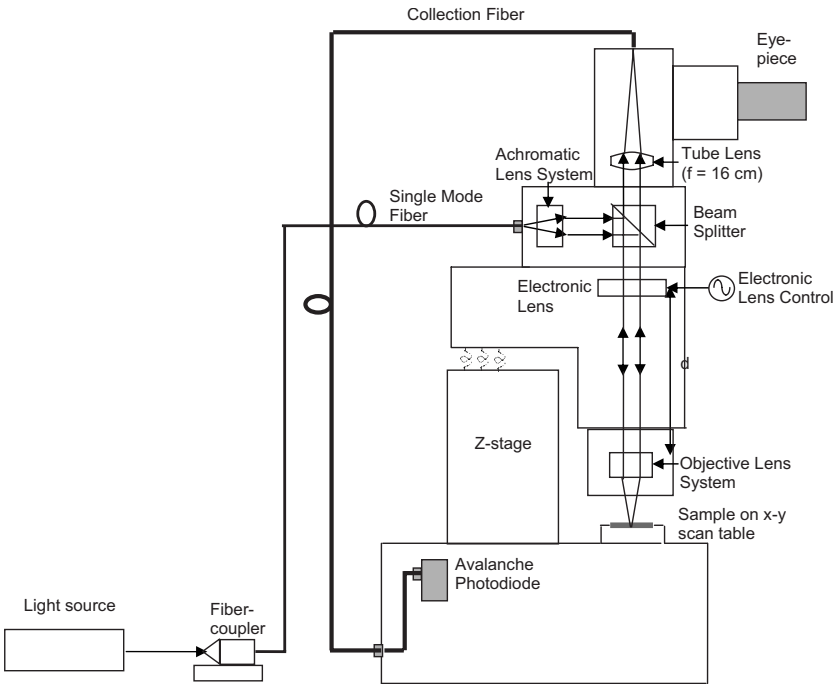

Fig. 1 Proposed electronic-lens-based axial-scanning 3-D imaging confocal microscope system realized by modifying a WITec AlphaSNOM 3-D imaging system.

cally controlled no-moving-parts optical beam 3-D scanners have been suggested to play a positive role in application-dependent scanning microscopy instruments.[22]

Continuing the same theme of wavelength-independent microscopy, recently proposed is the use of electronic optical scanning technology (e.g., LC and mirror-based methods) to alleviate the moving-parts scanning burden for confocal microscopes.[23] Independently, researchers have pursued using electronically controlled microelectromechanical system (MEMS) mirrors[24] and fluidic[25] lenses for scanning in optical coherence tomography (OCT) imagers, including the use of an acousto-optic electronically controlled cylindrical lens for axial scanning in multiphoton laser scanning microscopy.[26] LC e-lens technology can be used in a basic confocal microscopy setup to enable no-moving-parts axial scanning to realize depth-direction scans of electronic and optical materials in order to produce 1-D profile sections of a material.[27] Also shown is how the earlier developed LC e-lens-based confocal design can be applied to a full 3-D-scan commercial confocal and near-field microscopy system, a WITec AlphaSNOM.[28] The focus of the present paper is to provide the first step in acquiring and studying the 3-D imaging data from a blood-vessel slide sample viewed with the LC e-lens confocal microscope. The rest of the paper describes the proposed LC e-lens confocal microscopy system and its experimental results.

2 Proposed E-LENS-Based Axial-Scanning Confocal Microscope

The proposed confocal microscopy approach, shown in Fig. 1 in a reflection mode, uses the concept of a programmable weak thin lens cascading with a strong fixed focal length microscope objective lens to form a variable-focal-length objective. A transmission-mode system would involve an additional e-lens placed below the second objective under the sample.[23] A commercially available full 3-D scanning confocal microscope, the WITec AlphaSNOM, is modified by inserting a LC e-lens in its sample arm. The sample is illuminated using coherent light in the visible region of the electromagnetic spectrum. This light is coupled into a polarization-maintaining SMF using a fiber coupler, which is connected to the body of the microscope. This arrangement can be used to get either p- or s-polarized light inside the microscope body, depending on the polarization of the incident light and the direction in which the fiber is connected to the microscope body. This is important in order to have the light polarized along the director of a polarization-based e-lens such as a LC-material e-lens. Once inside the microscope body, the light is collimated using an achromatic lens system. In the sampling arm, the light passes through the e-lens and the objective lens system, placed a distance d apart from each other, and is focused onto the sample. The reflected light from the sample goes into the detection arm and is coupled into a collection fiber using a tube lens. The core of this collection fiber acts as the confocal pinhole and rejects the out-of-focus light. An avalanche photodiode in photon-counting mode is used as the detector, although a lower-cost pin photodiode can also be used in the system. The sample is scanned in the x and y directions using precision piezoelectric stages built into the microscope. However, in the axial (z) direction, the sample is fixed and scanning is achieved by just varying the drive signal of the e-lens.

Figure 2 further illustrates the difference between the standard confocal microscope and the e-lens-based confocal microscope. When the e-lens is used, the focal plane can be changed electronically by varying the drive signal.

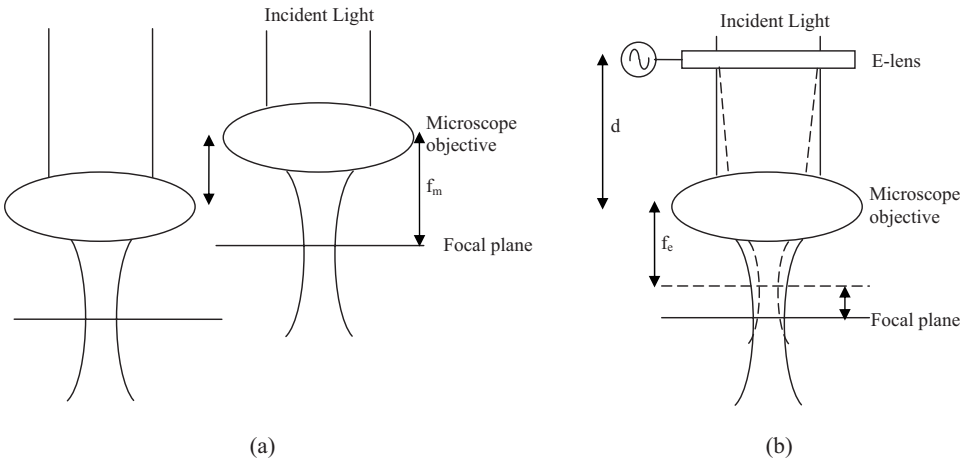

Fig. 2 Working principle of (a) standard confocal microscope with moving objective (or sample), (b) e-lens-based confocal microscope. Dashed lines show the modified beam path when the e-lens is turned on to change focus.

The e-lens adds weak positive lensing to the incident light, which is then focused onto a plane that is closer to the micro-objective lens than its original focal plane [see Fig. 2(b)]. The light from this new plane is then imaged onto the confocal pinhole. The axial scan range depends on the type of micro-objective used and on the effect of spherical aberrations introduced by the physical placement of the e-lens coupled to an optimized objective and the e-lens's nonideal wavefront control operations. For a higher (lower) numerical aperture (NA) of the micro-objective, the scan range is shorter (longer). Ideally, for an aberration-free objective-optimized confocal microscope using axial mechanical motion, the transverse and axial resolutions are given by[4]

$$d_{\mathrm{Tr}} = 0.46\frac{\lambda}{\mathrm{NA}}, \tag{1a}$$

$$d_{\mathrm{Ax}} = \frac{1.4n\lambda}{\mathrm{NA}^2}. \tag{1b}$$

Here λ is the wavelength of incident light, NA is the numerical aperture of the micro-objective, and n is the refractive index of the object medium. The e-lens and the micro-objective lens together form a two-lens system, the effective focal length f_e of which is given by

$$f_e = \left(\frac{1}{f_m} + \frac{1}{f_{el}} - \frac{d}{f_m f_{el}}\right)^{-1}. \tag{2}$$

Here f_m and f_{el} are the focal lengths of the microscope objective lens and the electronic thin lens, respectively, and d is the separation between the two lenses. The focal length f_m remains fixed, while f_{el} changes as the drive signal to the e-lens is changed. Note that the model in Fig. 2 is only a basic illustration of the e-lens varying-focal-length confocal microscope; in practice, a micro-objective assembly consists of several lenses instead of just one spherical lens.

3 Experimental Demonstration

For a first-step proof-of-concept experiment to demonstrate simple controlled biological sample imaging, the setup in Fig. 1 was realized by modifying a WITec AlphaSNOM confocal microscope by inserting an LC e-lens at a distance $d=5$ cm from the objective lens in the sample arm of the microscope. The LC e-lens used for our experiment is based on nematic liquid crystal (NLC) technology and enables microscope-objective focal-length changes via adjustment of the e-lens drive frequency. Details on this NLC e-lens and its effects on confocal microscopy parameters such as point spread functions (PSFs) and aberrations are described in Refs. 27 and 29. This e-lens has a 5-mm-diameter active lens area. Its focal length changes from infinity to 1 m for a frequency change from 0 to 60 kHz. The device uses a 25-μm-thick NLC layer sandwiched between glass layers making an 8-mm-thick optical device.

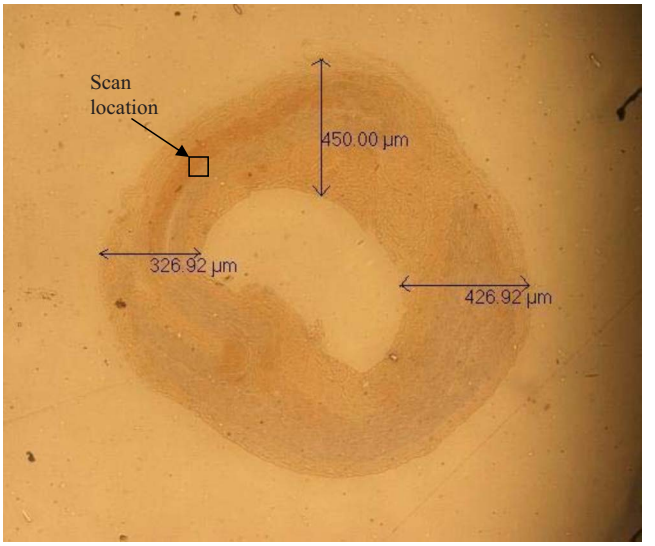

Fig. 3 Cross section of pig artery from CDC slide produced using standard optical microscope.

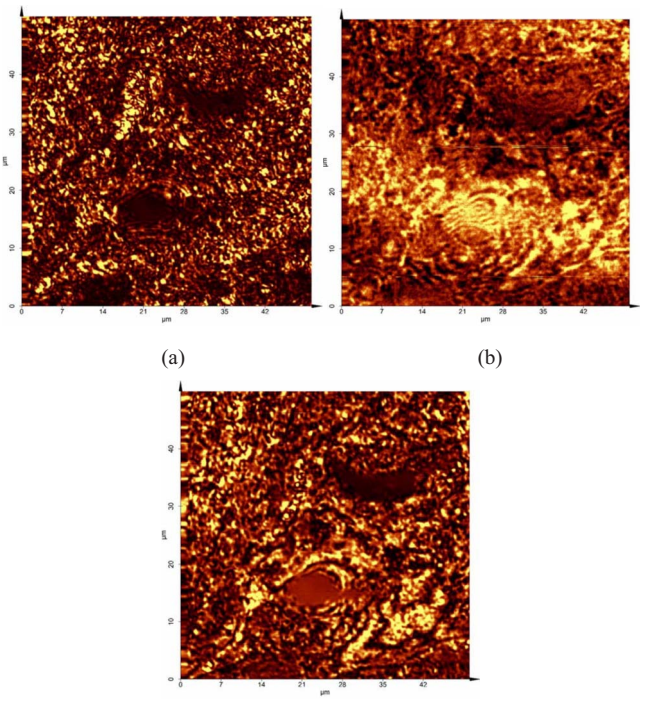

Fig. 4 Artery sample: 50×50-μm cross-sectional (transverse, *xy*) scan of 500×500 pixels with a 60× objective), using (a) conventional all-mechanical scan confocal microscope, (b) modified confocal microscope with NLC e-lens set for a 5-μm focal-length change, and (c) modified confocal microscope using 5-μm focus-change on-state e-lens and a counterdirection 5-μm axial (depth) scan position offset via mechanical motion to recover the image in (a).

The transmission of the device is ≈70% at 633 nm. The light source used is a MellesGriot 15-mW 633-nm He-Ne laser, which is coupled into a 4-μm SMF. A combination of various neutral-density filters is used between the laser and the fiber coupler to control the amount of light illuminating the sample. The tube lens used in the detection arm to focus the reflected light onto the confocal pinhole has a focal length $f=16$ cm. The core of the collection fiber has a diameter of 8 μm. Two different micro-objectives, a 60× (NA=0.8) and a 20× (NA=0.4), are used to get two different sets of data as explained in the following paragraphs.

Figure 3 shows a cross-sectional view and dimensions of an approximately two-month-old pig artery in a Center for Disease Control (CDC) slide No. IHC04-115, Hemediagnostic S-100D. 3-D images [i.e., *xy* transverse images at different *z* (axial) scan locations, and *xz* and *yz* scans] of this pig artery have been realized using both the conventional all-mechanical scanning confocal microscope and the modified NLC e-lens-based confocal microscope, using a 60× (NA=0.8) micro-objective. Figure 4 shows transverse (cross-sectional) views of the marked square targeted area in Fig. 3. The scans in Fig. 4 are 500×500 pixels with a motion step of 0.1 μm, enabling a 50×50-μm imaged zone. The data for Fig. 4(a) were obtained by using the mechanical *z*-stage motion to position the confocal depth at a chosen position within the artery. Next, with the mechanical *z* stage at the same location, the NLC e-lens was turned on for a 5-μm focal shift (≈3.5 axial imaging bins—i.e.

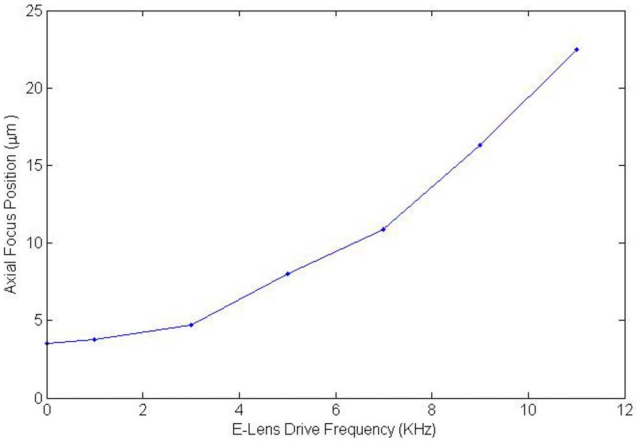

Fig. 5 Example measured change in axial focus position in the NLC e-lens confocal microscope with a 60× (NA=0.8) micro-objective for selected e-lens drive frequencies up to 11 kHz.

focal-depth increments), and a transverse scan was taken [see Fig. 4(b)]. The change in focus caused by the e-lens is clearly visible. With the e-lens still on, data for Fig. 4(c) were obtained by moving the mechanical *z* stage by 5 μm to recover the desired known axial location and then performing a mechanical cross-sectional scan. As expected, Fig. 4(a) and Fig. 4(c) are visually similar.

The data for Fig. 5 were acquired with a gold mirror as a sample target and using the calibrated axial motion stage of the WITec AlphaSNOM microscope. With this experimental arrangement incorporating the high-NA (0.8), 60× micro-objective, a total scan range of 19 μm was measured using e-lens drive frequencies up to 11 kHz. The deployed e-lens can also be driven at frequencies up to 60 kHz, which results in a higher scan range, e.g., 125 μm, although at the cost of larger spherical aberrations.

In the second part of the experiment, the 60× micro-objective was replaced with a 20× (NA=0.4) micro-objective. Figure 6 shows a white-light image of the sample

Fig. 6 White-light image of pig artery produced using the WITec AlphaSNOM with a 20× micro-objective. The square zone is the 80×80-μm area imaged in Fig. 7.

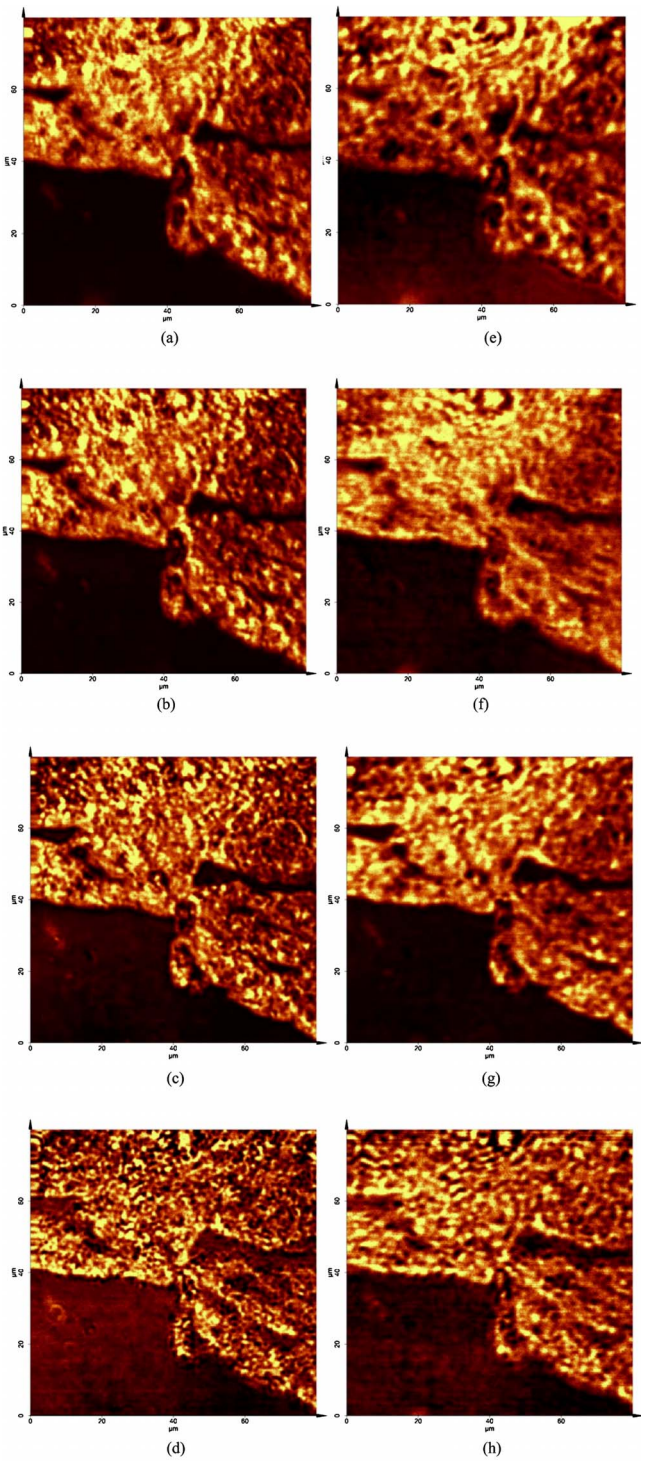

Fig. 7 Artery sample: 80×80 μm cross-sectional (transverse, *xy*) scan of 400×400 pixels with a 20× objective using conventional all-mechanical scan confocal microscope at axial scan locations Δz of (a) 0, (b) 5, (c) 15, and (d) 25 μm, and using modified confocal microscope with NLC e-lens set for focal-length changes of (e) 0, (f) 5, (g) 15, and (h) 25 μm.

along with the marked 80×80-μm targeted area that is imaged by the microscope. This time the targeted area is along the edge of the artery. Transverse images at four different axial locations (Δz=0, 5, 15, and 25 μm) were taken using the standard microscope and the modified e-lens microscope shown in Fig. 7(a)–7(d) and 7(e)–7(h), respectively. These scans are 400×400 pixels, taken with a motion step of 0.2 μm in the lateral direction. For the standard microscope, the axial locations are varied by mechanically moving the micro-objective lens; for the e-lens-based microscope, the sample and the micro-objective are fixed and only the drive signal to the NLC e-lens is varied. The corresponding scans, shown side by side in Fig. 7, are similar to each other, thereby showing the first-step proof-of-concept 3-D imaging results of this system. A quantitative analysis showing the similarity between these scans is undertaken in Section 4. Note that the scan range in this case is a factor of ≈2.5 greater than the corresponding scan range with a 60× micro-objective. The electronic and mechanical axial-direction scanning were over a 25-μm zone that was more than adequate to scan the pig artery.

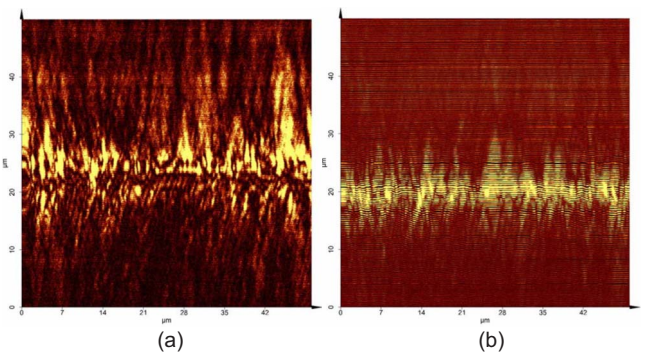

Fig. 8 Artery sample: 50×50-μm axial (*xz*) scan of 500×500 pixels with a 60× objective taken at *y*-scan location *y*=0 μm, using (a) conventional all-mechanical-scan confocal microscope and (b) modified confocal microscope using NLC e-lens set for a 5-μm focal-length change. Vertical axis is the *z* axis, and horizontal axis is the *x* axis.

Figure 8 shows example 500×500-pixel *xz* axial scan data obtained using the 60× (NA=0.8) objective with an *x*-motion step of 0.1 μm and a *z*-motion step of 0.1 μm. Figure 8(a) shows *xz* axial scan data using the standard motion-based WITec AlphaSNOM, while Fig. 8(b) shows *xz* axial scan data using the e-lens-based system. The Fig. 8 data show that the whole blood vessel is around 25 μm thick. Using the e-lens, the scan in Fig. 8(b) was displaced by 5 μm in the *z* direction from the scan in Fig. 8(a). Compared to Fig. 8(a), Fig. 8(b) shows a drop in acquired axial-scan light levels, because the optical power, at the axial focus position, as shown earlier, decreases as the e-lens focusing power increases.[27] Also note that the addition of the e-lens has resulted in horizontal stripes in the image. This is most likely the result of reflections introduced inside the microscope by the e-lens, which might be eliminated by using an antireflective coating on the e-lens.

Figure 9 shows the axial scans taken with the e-lens set for various larger focal-length changes, resulting in larger *z* displacements than in Fig. 8(a). One can clearly observe the changing *z* position of the blood artery as the e-lens changes its focusing power.

The present NLC e-lens takes a rather long time (1 s) reset. Nevertheless, these slow NLC e-lenses can be cascaded in a digital LC lens design, shown earlier in Ref. 30, that can lead to a much shorter (e.g., 1 μs) reset time, en-

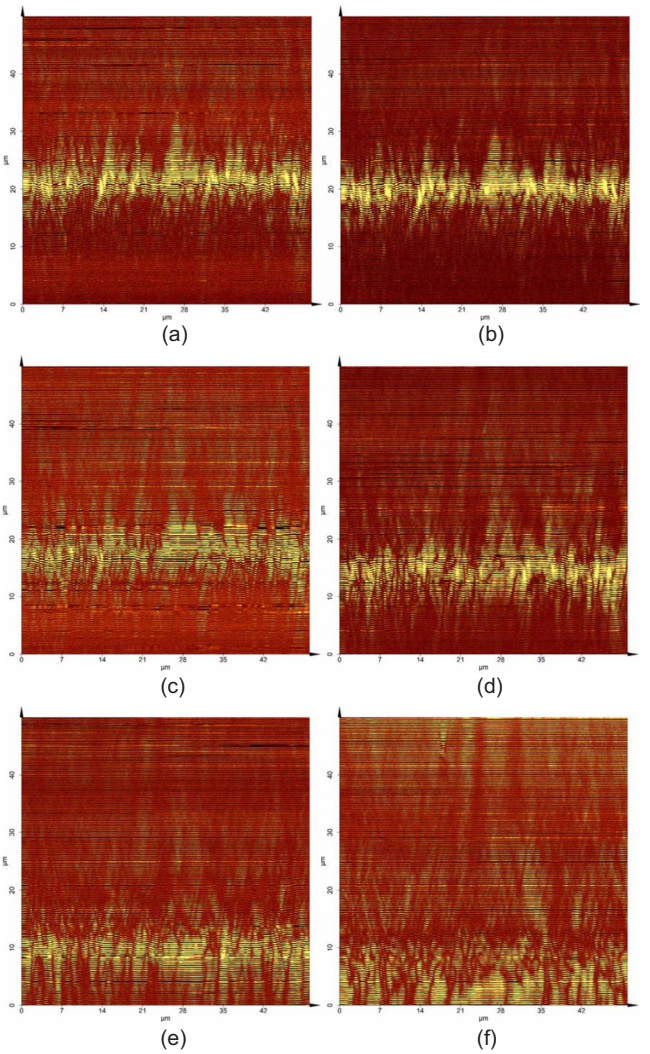

Fig. 9 Artery sample: 50×50-μm axial (xz) scan of 500×500 pixels with a 60× objective taken at y-scan location $y=0$ μm, using a NLC e-lens set for focal-length changes of (a) 4, (b) 5, (c) 8, (d) 11, (e) 16, and (f) 22.5 μm. The vertical and horizontal axes correspond respectively to the z axis and the x axis.

abling capture of fast temporal effects in biological samples such as neurons. Hence, the use of a single NLC lens as described in this paper is only a first step in achieving a fast e-lens confocal microscope design.

4 Data Analysis

In the previous work using this NLC e-lens in a confocal microscope, typical confocal microscopy conditions were examined, such as operation with and without e-lens axial PSFs, and measured system transverse resolution in the presence and absence of e-lens operation using a sample with given resolution (viz., an optical waveguide chip).[27] These 3-D imaging results on a homogeneous material (indium phosphide) optical chip indicated comparable performance of the systems without and with the e-lens, in view of the presence of e-lens spherical aberrations due to NLC lens performance and optical design of the e-lens, in contrast with the aberration-optimized objective lens.[27] Given these positive results, the next step in the experimentation was to deploy a typical inhomogeneous (nonspecular) material sample such as a biological sample, viz., the pig artery in a glass slide. Section 3 has presented some axial scans of this blood vessel: Fig. 4 and Fig. 7 show xy (transverse) scans at selected axial (z) scan locations. Since the scans are from a biological sample with unknown internal 3-D structure, a possible method, commonly used in computer vision engineering, is correlation of images by computer-based image processing. Thus, here too, as a first step, we deployed the image correlation technique to compare the axial scans obtained via the mechanical-motion and the E-lens WITec AlphaSNOM.

The 2-D normalized cross-correlation function between two images $f(x,y)$ and $g(x,y)$ is given as[31]

$$r(u,v)=\frac{\sum_{x,y}[f(x,y)-\bar{f}][g(x-u,y-v)-\bar{g}]}{\{\sum_{x,y}[f(x,y)-\bar{f}]^2\}^{1/2}\{\sum_{x,y}[g(x-u,y-v)-\bar{g}]^2\}^{1/2}}, \tag{3}$$

where $\bar{f}$ and $\bar{g}$ are the respective mean values of the two images. The values of this function are bounded between -1 and 1, with a value of 1 denoting maximum positive correlation when $f(x,y)=g(x,y)$ and $u=0$, $v=0$. A value of 0 indicates no correlation, while a value of -1 indicates a negative correlation implying $f(x,y)=-g(x,y)$.

The Fig. 7 images taken from the standard WITec microscope and from the modified NLC e-lens microscope are correlated against each other to determine as a first step the quality of our experimental results. The correlation results for each of the four locations of the blood vessel are shown in Fig. 10. The results show high peak correlation values of 0.91, 0.86, 0.90, and 0.81 for focal shifts of 0, 5, 15, and 25 μm, respectively. These preliminary results show that the blood artery information taken at different axial (z) scan locations using the NLC e-lens confocal microscope are reasonably similar to the data taken using the standard mechanical motion microscope. Figure 11 shows similar correlation data for the Fig. 4 data. Specifically, Fig. 11(a) shows the autocorrelation (peak value=1) of the mechanically in-focus data, i.e., Fig. 4(a). Figure 11(b) shows the cross-correlation between the mechanically in-focus data of Fig. 4(a) and the out-of-focus data of Fig. 4(b) produced by controlling the NLC lens. The cross-correlation peak is 0.64. On the other hand, Fig. 11(c) shows the cross-correlation between the mechanically in-focus data of Fig. 4(a) and the NLC e-lens in-focus data of Fig. 4(c) with a cross-correlation peak of 0.71. These autocorrelation and cross-correlation data give a preliminary indication of the level of performance achieved by the demonstrated e-lens-based microscopy system.

It is important to point out that better parameters to quantify the biological 3-D microscopy performance are the axial and transverse PSFs, and this will be attempted in a future experiment using defined 3-D targets such as various sizes of metal beads in a scattering medium.

The departure of these preliminary data correlation values from the ideal value of 1 is primarily due to optical aberrations introduced into the system by the presence and

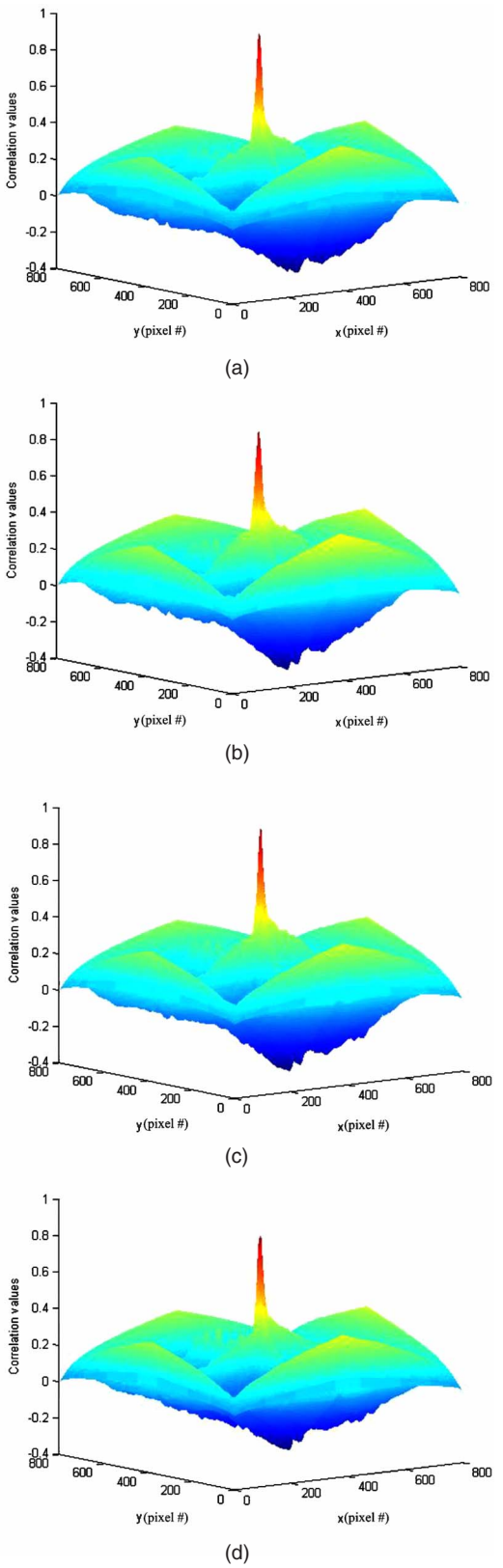

Fig. 10 Cross-correlation results between Fig. 7 data scans taken using the standard confocal microscope and the e-lens confocal microscope at Δz scan locations of (a) 0, (b) 5, (c) 15, and (d) 25 μm.

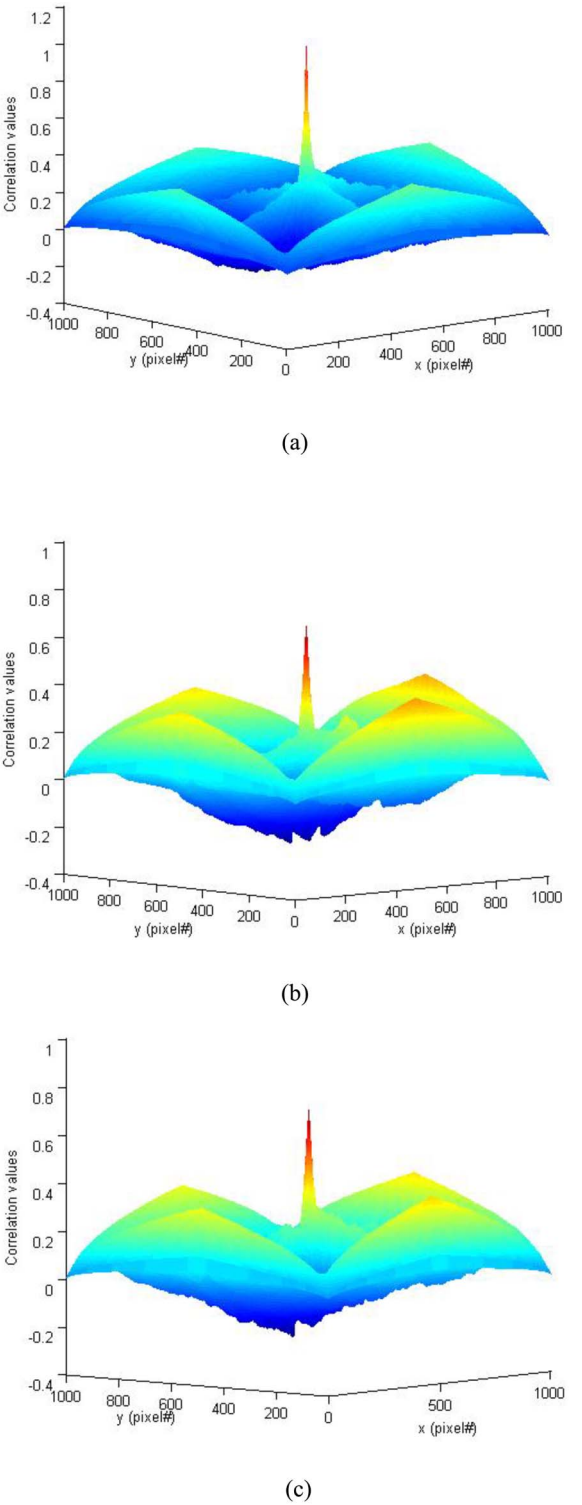

Fig. 11 (a) Autocorrelation of Fig. 4(a) in-focus data scan, (b) cross-correlation of Fig. 4(a) in-focus data scan and Fig. 4(b) NLC e-lens out-of-focus data scan, and (c) cross-correlation of Fig. 4(a) in-focus data scan and Fig. 4(c) NLC e-lens in-focus data scan.

operation of the e-lens. The most significant aberration caused by this NLC e-lens is spherical aberration[29] and is primarily caused by the nonlinear part of the electro-optic response of the LC. This aberration is not uniform over the aperture of the lens and in fact changes sign as we move

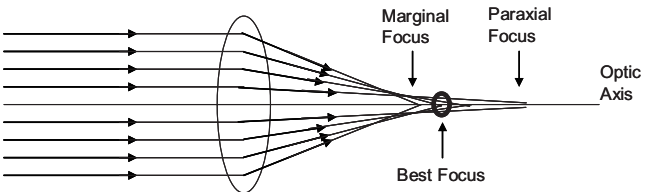

Fig. 12 Difference between the Gaussian image point and the point of best focus in the presence of spherical aberration in an imaging system.

from the center to the edge of the lens. It is also different for different values of the drive signal (for focus change). Note that each micro-objective is carefully designed for optimal focus, i.e., a Gaussian focus point when using a collimated, plane-wave input beam. By placing an e-lens before the micro-objective entrance face, one deviates from this optimal condition by introducing spherical wavefronts into the objective. These spherical wavefronts add to the already present spherical aberration, due to e-lens imperfection, in the overall imaging system.

When no spherical aberration is present in an imaging system, all rays are focused to a single point, known as the Gaussian image point. However, in the presence of spherical aberration, rays away from the optic axis are focused at slightly different locations from the rays close to the optic axis (see Fig. 12). The point where the rays close to the optic axis are focused is known as the *paraxial focus* or Gaussian image point, while the point where rays close to the edge of the lens are focused is known as the *marginal focus*. The point of best focus (commonly known as the *circle of least confusion*) is defined as the point where the resultant focused optical blur spot is the smallest and occurs somewhere in between the paraxial and the marginal foci.[32] The size of this smallest optical spot is larger than the corresponding smallest optical spot in the absence of any spherical aberration. With respect to the proposed e-lens-based microscope, a point to note is that instead of the point of best focus, the Gaussian image point is still being imaged onto the confocal pinhole. This is what causes the decrease in lateral resolution as evidenced by the slight blurring of the data features as seen in the scans taken using the e-lens-based microscope. An important point to notice here is that this aberration will be less for low-NA micro-objectives than for high-NA ones, since for a high-NA lens, the beam expands more rapidly beyond the point of best focus. It is worth remembering that when the NLC e-lens is turned on, the Gaussian image point itself moves according to the drive signal of the e-lens, and at each value of the drive signal, a different Gaussian image point is being focused on the confocal pinhole. We refer to this phenomenon as focus change caused by the function of the e-lens. Other aberrations such as coma, tilt, and astigmatism, as documented in Ref. 29 for this NLC E-lens, are not as significant as the spherical aberration effect.

One possible option for compensating these spherical aberrations is by adding an appropriate amount of defocus to the system,[33] so as to image the point of best focus instead of imaging the Gaussian image point onto the confocal pinhole. What makes this task challenging is the variable nature of the aberration, i.e., the amount of aberration changes with varying amounts of focus change caused by the e-lens. Hence, one needs to use an adaptive method of introducing defocus into the imaging system. One such method could be the introduction of another e-lens in the detection arm.[23] This second e-lens could be used in conjunction with the tube lens to focus light coming from the plane of best focus onto the detection pinhole instead of the light coming from the Gaussian image point. The synchronized drive signals to the two e-lenses would need to be carefully optimized in order to compensate for the axial-scan-position spherical aberration with an opposite amount of defocus aberration.

Another well-known approach to counter spherical aberrations in an optical microscope is by the use of an adaptive spatial light modulator such as a 2-D deformable mirror device that can be electronically programmed to produce the desired wavefront correction.[34,35] In any case, it is important to stress that spherical aberrations due to the e-lens-based confocal microscope design must be adequately compensated to realize the true potential of quality 3-D imaging.

5 Conclusion

We have demonstrated the use of an NLC e-lens in a confocal microscope to produce 3-D imaging of a sample blood vessel in a glass slide. The e-lens allows a no-moving-parts focus change in the biological sample. Such an e-lens-based design can lead to elimination of mechanical forces on test samples, which occur when fast mechanical axial motion between objective and sample is introduced as in conventional confocal microscopes. The performance of the e-lens-based confocal microscope will greatly depend of the type of e-lens technology employed (e.g., NLC, MEMS, liquid), given that each e-lens type has different levels of aberration performance.[36–38] Future work will relate to quantifying aberration and 3-D imaging performance using known 3-D targets in scattering media.

Acknowledgments

We thank Dr. Sajjad Khan for initial experimental support, and Amana Bokhari-Riza of Nuonics, Inc., for original insights. In addition, we thank Professor Chang-Huei Yang of Caltech for providing the CDC blood vessel slide.

References

1. M. Minsky, "Microscopy apparatus," U.S. Patent No. 3,013,467 (1961).
2. T. Wilson, *Confocal Microscopy*, Academic Press, San Diego (1990).
3. T. Corle and G. Kino, *Confocal Scanning Optical Microscopy and Related Imaging Systems*, Academic Press, San Diego (1996).
4. M. Rajadhyaksha, R. Anderson, and R. Webb, "Video-rate confocal scanning laser microscope for imaging human tissues in vivo," *Appl. Opt.* **38**(10), 2105–2115 (1999).
5. R. L. Forward, "Passive beam deflecting apparatus," U.S. Patent No. 3,612,659 (1971).
6. G. Molesini, G. Pedrini, P. Poggi, and F. Quercioli, "Focus wavelength encoded optical profilometer," *Opt. Commun.* **49**(4), 229–233 (1984).
7. M. A. Browne, O. Akinyemi, and A. Boyde, "Confocal surface profiling using chromatic aberration," *Scanning* **14**, 145–153 (1992).
8. B. Picard, "Method for the scanning confocal light optical microscopic & indepth examination of an extended field & devices for implementing said method," U.S. Patent No. 4,965,441 (1990).
9. H. J. Tiziani and H. M. Uhde, "Three dimensional image sensing by chromatic confocal microscopy," *Appl. Opt.* **33**(10), 1838–1843 (1994).

10. N. A. Riza, "Photonically controlled ultrasonic arrays: scenarios and systems," in *IEEE Ultrasonics Symp.*, Vol. **2**, pp. 1545–1550 (1996).
11. N. A. Riza, "Photonically controlled ultrasonic probes," U.S. Patent No. 5,718,226 (1998).
12. G. J. Tearney, R. H. Webb, and B. E. Bouma, "Spectrally encoded confocal microscopy," *Opt. Lett.* **23**(15), 1152–1154 (1998).
13. N. A. Riza and Y. Huang, "High speed optical scanner for multi-dimensional beam pointing and acquisition," in *IEEE LEOS Annual Meeting*, Vol. **1**, pp. 184–185 (1999).
14. N. A. Riza and Z. Yaqoob, "High-speed fiber-optic probe for dynamic blood analysis measurements," *Proc. SPIE* **4163**, 18–23 (August 2000).
15. Z. Yaqoob, A. A. Rizvi, and N. A. Riza, "Free-space wavelength multiplexed optical scanner," *Appl. Opt.* **40**(35), 6425–6438 (2001).
16. Z. Yaqoob and N. A. Riza, "Free-space wavelength-multiplexed optical scanner demonstration," *Appl. Opt.* **41**(26), 5568 (2002).
17. G. J. Tearney, M. Shishkov, and B. E. Bouma, "Spectrally encoded miniature endoscopy," *Opt. Lett.* **27**(6), 412–414 (2002).
18. Z. Yaqoob, M. Arain, and N. A. Riza, "Wavelength multiplexed optical scanner using photothermorefractive glasses," *Appl. Opt.* **42**(26), 5251 (2003).
19. Z. Yaqoob and N. A. Riza, "Low loss wavelength-multiplexed optical scanners using volume Bragg gratings for transmit-receive lasercom systems," *Opt. Eng.* **43**(5), 1128–1135 (2004).
20. N. A. Riza, "Wavelength switched fiber-optically controlled ultrasonic intracavity probes," in *IEEE LEOS Ann. Mtg. Digest*, pp. 31–36 (1996).
21. Z. Yaqoob and N. A. Riza, "High-speed scanning probes for internal and external cavity biomedical optics," in *OSA Biomedical Topical Meeting*, pp. 381–383 (2002).
22. N. A. Riza, "Multiplexed optical scanner technology," U.S. Patent No. 6,687,036 (2004).
23. N. A. Riza and A. Bokhari, "Agile optical confocal microscopy instrument architectures for high flexibility imaging," in *Three Dimensional Confocal Microscopies, BIOS 2004 Biomedical Optics, Photonics West, Proc. SPIE* **5324**, 77–88 (Jan. 2004).
24. B. Qi, A. P. Himmer, L. M. Gordon, X. D. V. Yang, L. D. Dickensheets, and I. A. Vitkin, "Dynamic focus control in high-speed optical coherence tomography based on a microelectromechanical mirror," *Opt. Commun.* **232**(1–6), 123–128 (2004).
25. A. Divetia, T. Hsieh, J. Zhang, Z. Chen, M. Bachman, and G. Li, "Dynamically focused optical coherence tomography for endoscopic applications," *Appl. Phys. Lett.* **86**, 103902 (2005).
26. G. D. Reddy and P. Saggau, "Fast three-dimensional laser scanning scheme using acousto-optic deflectors," *J. Biomed. Opt.* **10**(6), 064038 (2005).
27. S. A. Khan and N. A. Riza, "Demonstration of a no-moving-parts axial scanning confocal microscope using liquid crystal optics," *Opt. Commun.* **265**(2), 461–467 (2006).
28. N. A. Riza, M. Sheikh, G. Webb-Wood, and P. Kik, "Demonstration of three dimensional imaging of blood vessel using a no-moving parts electronic lens-based optical confocal microscope," in *Conf. MI03: Physics of Medical Imaging, SPIE Medical Imaging, Proc. SPIE* **6510**, 65100J1–5 (Feb. 2007).
29. G. Vdovin, A. Naumov, M. Loktev, V. Belopukhov, F. Vladimirov, and G. Love, "Wave front control systems based on modal liquid crystal lenses," *Rev. Sci. Instrum.* **71**(9), 3290–3297 (2000).
30. N. A. Riza and S. A. Khan, "Polarization multiplexed optical scanner," *Opt. Lett.* **28**(7), 561–563 (2003).
31. R. C. Gonzalez and R. E. Woods, *Digital Image Processing*, 3rd ed., Addison-Wesley, Reading, MA (1992).
32. M. Gu and C. J. R. Sheppard, "Effects of defocus and primary spherical aberration on three-dimensional coherent transfer functions in confocal microscopes," *Appl. Opt.* **31**(14), 2541–2549 (1992).
33. V. Mahajan, "Axial irradiance of a focused beam," *J. Opt. Soc. Am. A* **22**(9), 1814–1823 (2005).
34. L. Sherman, J. Y. Ye, O. Albert, and T. B. Norris, "Adaptive correction of depth-induced aberrations in multiphoton scanning microscopy using adeformable mirror," *J. Microsc.* **206**(1), 65–71 (2002).
35. Y. Yasuno, T. F. Wiesendanger, A. K. Ruprecht, S. Makita, T. Yatagai, and H. J. Tiziani, "Wavefront-flatness evaluation by wavefront-correlation-information-entropy method and its application for adaptive confocal microscope," *Opt. Commun.* **232**(1–6), 91–97 (2004).
36. S. Kuiper and B. H. W. Hendriks, "Variable-focus liquid lens for miniature cameras," *Appl. Phys. Lett.* **85**, 1128–1130 (Aug. 16, 2004).
37. B. Berge and J. Peseux, "Variable focal lens controlled by an external voltage: an application of electrowetting," *Eur. Phys. J. E* **3**, 159–163 (2000).
38. G. Vdovin, P. M. Sarro, and S. Middelhoek, "Technology and applications of micromachined adaptive mirrors," *Opt. Eng.* **36**(5), 1382–1390 (1997).

Biographies and photographs of the authors not available.